The Astrophysical Journal, 761:189 (5pp), 2012 December 20 doi:10.1088/0004-637X/761/2/189

ERRATUM: "VERTICAL STRUCTURE OF A SUPERNOVA-DRIVEN TURBULENT, MAGNETIZED INTERSTELLAR MEDIUM" (2012, ApJ, 750, 104)

Alex S. Hill[1,7], M. Ryan Joung[2,3], Mordecai-Mark Mac Low[3], Robert A. Benjamin[4], L. Matthew Haffner[1], Christian Klingenberg[5], and Knut Waagan[6]
[1] Department of Astronomy, University of Wisconsin-Madison, Madison, WI, USA; alex.hill@csiro.au
[2] Department of Astronomy, Columbia University, New York, NY, USA
[3] Department of Astrophysics, American Museum of Natural History, New York, NY, USA
[4] Department of Physics, University of Wisconsin-Whitewater, Whitewater, WI, USA
[5] Department of Mathematics, Würzburg University, Emil Fischer Strasse 30, Würzburg, Germany
[6] Department of Applied Mathematics, University of Washington, Seattle, WA, USA
Received 2012 November 2; published 2012 December 6

Key words: Galaxy: disk – Galaxy: structure – ISM: kinematics and dynamics – ISM: structure – magnetohydrodynamics (MHD) – turbulence

1. SIMULATIONS

Due to an error in the code, the heating and cooling in the simulations we presented in the published paper (Hill et al. 2012) were not treated as described in the paper. We only applied the cooling ($-n^2\Lambda$) and diffuse heating ($n\Gamma$) terms in Equation (3) of the paper in timesteps in which supernovae occurred. The stellar wind heating was also only applied in timesteps in which supernovae occurred (if stellar wind heating was appropriate, as described in the text). Typical timesteps are $\Delta t \sim 10^{-3}$ Myr, though this value changes by factors of more than 10 over the course of the simulation and is typically lower in the unmagnetized case and highest in the most strongly magnetized case. The total (core-collapse plus Type Ia) supernova rate is 33.98 $\mathrm{Myr}^{-1}\,\mathrm{kpc}^{-2}$, so with our 1 kpc^2 box at the Galactic supernova rate employed in this work there is a supernova every ∼30 timesteps.

These errors in the code were introduced in the development of the high supernova rate models for Joung et al. (2009). Because this version of the code was only used for the 512× model in Joung et al. (2009) and supernovae occurred in nearly every timestep in those models, the effects of this error were minor in that work.

We have corrected these errors in the code and run replacement versions of the 3.90 pc midplane resolution `bx0`, `bx50`, and `bx100` simulations from initialization at 0 Myr to 340, 360, and 340 Myr, respectively. We have also evolved the 1.95 pc midplane resolution `bx0hr` and `bx50hr` simulations described in Hill et al. (2012) with the revised heating and cooling from 300 Myr to 320 Myr. Based on these new simulations, we present corrected versions of Figures 3, 5, 7, 8, 11, 13, and 14(b) and discuss the main implications of our error in Section 2. Our conclusion number 7, that the transition-temperature gas dominates by volume in the range 1 kpc $\lesssim |z| \lesssim$ 2.5 kpc, was due to the unphysical balance of cooling and shock heating and is invalid. The impact of the error on our remaining conclusions is relatively minor.

2. IMPLICATIONS

We present images of a vertical snapshot of the revised simulation in Figure 3. Because our error affected the cooling ($n^2\Lambda$) and diffuse heating ($n\Gamma$) terms in Equation (3) equally, the net heating in gas in which the diffuse heating dominates was not affected. Therefore, the basic structure of the warm and cold temperature regimes described in the paper was not significantly affected. As in the original runs, the vertical stratification is similar in the magnetized and unmagnetized simulations.

The major difference is in the transition-temperature ($10^{4.2}$ K $\lesssim T \lesssim 10^{5.5}$ K) gas. Because of the unphysical balance between shock heating and cooling, much of the volume was filled with thermally unstable transition-temperature gas in the original runs. As is evident in the revised Figure 3, the corrected runs feature sharp transitions from thermally stable warm ($T \sim 10^4$ K) gas to hot ($T \sim 10^6$ K) gas with a long cooling time. This transition typically occurs at $|z| \sim 1$ kpc, although the height varies widely both spatially and temporally due to interacting gas flows in each phase. In the revised simulations, it is warm, not transition-temperature, gas that dominates by volume at these heights (Figure 11).

The clear separation into a multi-phase interstellar medium (ISM) remains evident in mass-weighted probability distribution functions in Figure 5. In the published paper, we noted that a significant amount of gas cooled to the minimum temperature (10 K), as was evident in Figures 5 and 14(b); that effect is significantly reduced in the corrected simulations.

The thermal pressure–density phase diagram in Figure 14(b) shows that cold, cool, and warm gas is more tightly restricted to the thermally stable temperature curve in the revised simulations; because of the reduced diffuse heating and cooling times, gas that is perturbed away from thermally stable temperatures due to mixing returns to equilibrium quickly.

[7] Present address: CSIRO Astronomy and Space Science, Marsfield, NSW, Australia.

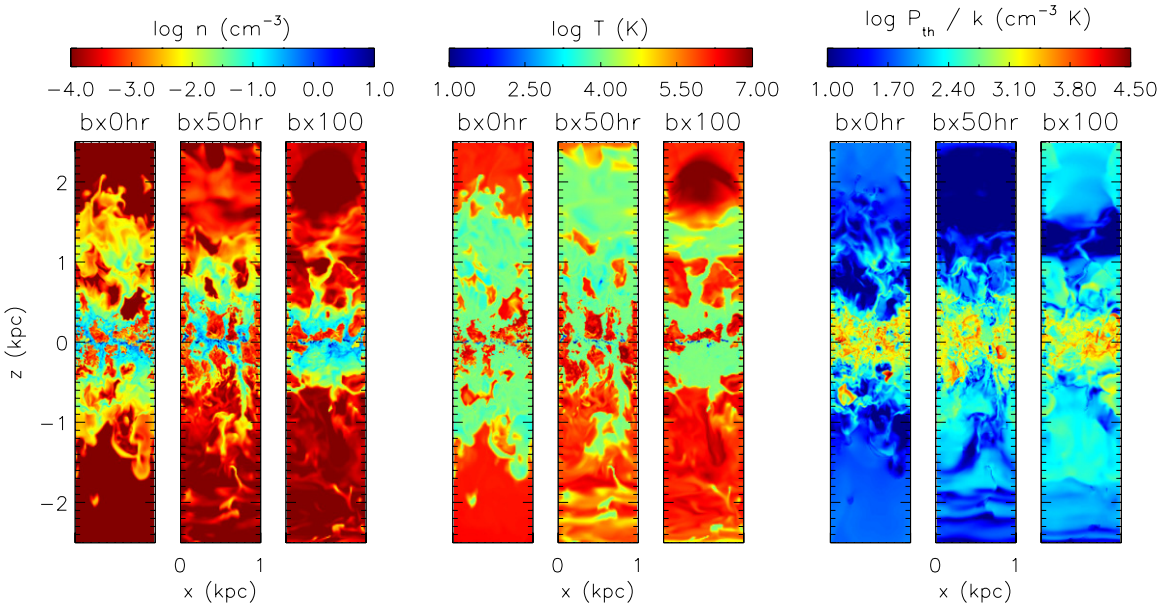

Figure 3. Vertical snapshots of density, temperature, and thermal pressure at $t = 320$ Myr from models with a range of initial magnetic field strengths (see Table 2 of the original paper). Slices from each model along the field are shown.

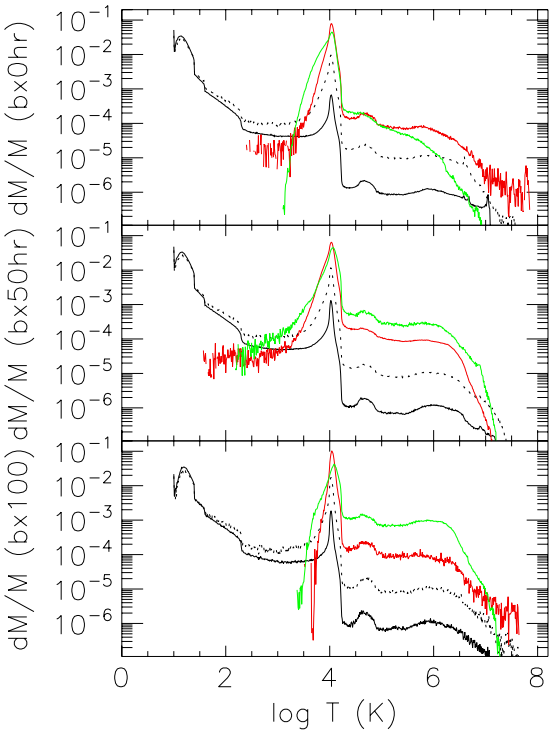

Figure 5. Mass-weighted histograms of temperature averaged over three time slices from $t = 318$–320 Myr in the corrected `bx0hr`, `bx50hr`, and `bx100` models (top to bottom). Histograms are calculated within specified height ranges: black solid lines: $|z| < 20$ pc; black dotted lines: $|z| < 500$ pc; red lines: 400 pc $< |z| <$ 600 pc; and green lines: 800 pc $< |z| <$ 1200 pc. Histograms were calculated with logarithmic bin intervals $d(\log T) = 0.01$.

Because of the increased cooling efficiency, the thermal energy in the revised run reaches a dynamical equilibrium value of $\approx 1 \times 10^{46}$ erg pc^{-2}, as shown in Figure 13; in the original runs, the thermal energy surface density was approximately twice this value. As in the original runs, the magnetic energy surface density approaches a value approximately one-third of the thermal energy surface density but is not clearly in a statistical steady-state by the end of the runs.

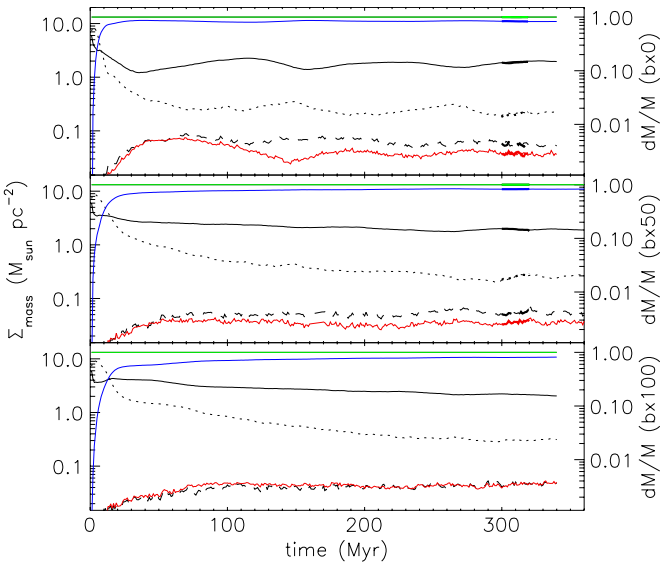

Figure 7. Surface mass density as a function of time for the corrected `bx0`, `bx50`, and `bx100` models (top to bottom), shown with thin lines. The corresponding high-resolution models, `bx0hr` and `bx50hr`, are overplotted with thick lines. The right axis indicates the corresponding mass fraction. The color and line styles are the same in all plots. Blue lines: $T < 200$ K. Dotted lines: 200 K $< T <$ 5000 K. Black solid lines: 5000 K $< T < 10^{4.2}$ K. Dashed lines: $10^{4.2} < T < 10^{5.5}$ K. Red lines: $T > 10^{5.5}$ K. Green lines: all gas.

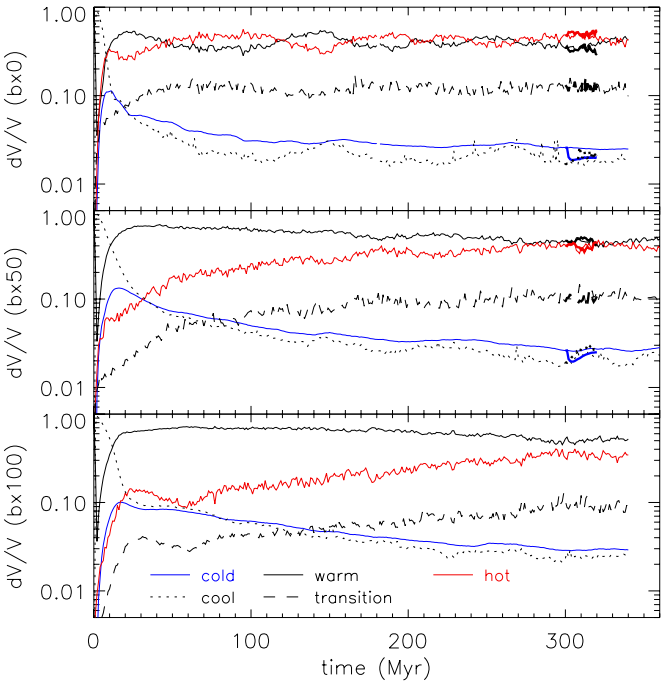

Figure 8. Time evolution of volume filling fractions of phases of the ISM, selected by temperature, in the plane ($|z| < 125$ pc). Plots are shown for all three models with the same line styles as in Figure 7.

We show mass and volume filling fractions of each phase as a function of time in Figures 7 and 8, respectively. As in the original simulations, the mass fraction in each phase is essentially the same in the 4 pc (thin lines) and 2 pc (thick lines) runs. Also as in the original simulations, the volume filling fractions are essentially the same for the phases which dominate by volume, though the cold gas filling fraction reduces from ≈0.03 to ≈0.02 when the resolution is increased. In all runs, the fraction of gas mass contained in the cold regime increased from ≈0.6 in the original runs to ≈0.8 in the revised runs, with a corresponding decrease in the mass in the warm regime. This is higher than the best estimate of the observed $T < 200$ K mass fraction in the solar neighborhood of the Milky Way of ≈0.55 (Ferrière 2001), suggesting that our simulations contain either more cooling or less heating than is present in the

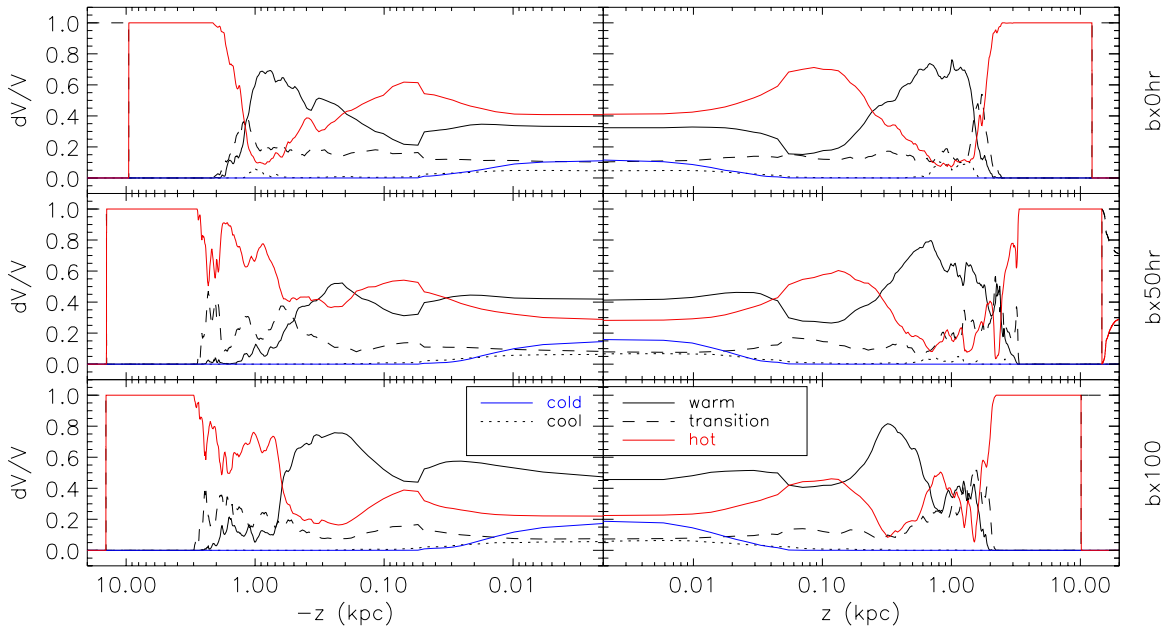

Figure 11. Volume filling fraction as a function of height for the `bx0` and `bx50` models (top to bottom) after 320 Myr. Line styles and colors are the same as in Figures 7 and 8. Note that the horizontal (z) axis scale is logarithmic.

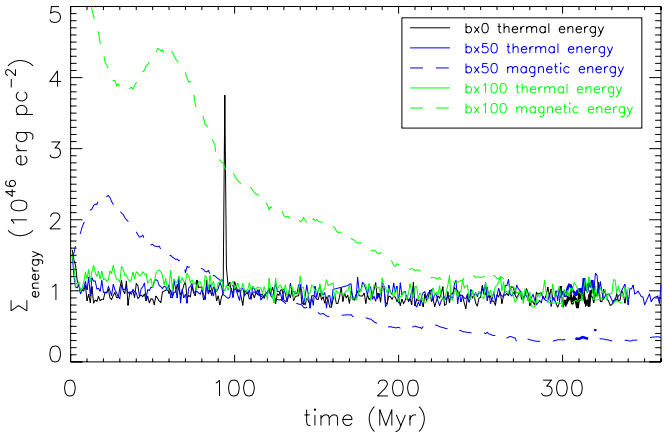

Figure 13. Surface magnetic (dashed lines) and thermal (solid lines) energy density as a function of time. The unmagnetized `bx0` and magnetized `bx50` and `bx100` models are shown with thin lines, while the high-resolution counterparts (`bx0hr` and `bx50hr`) are shown with thick lines.

cold and warm gas in the ISM. Thus, an additional heating mechanism not included in our models, such as photoionization heating (Reynolds et al. 1999), may be important.

The cold gas mass fraction found in our revised simulations is notably higher than the 0.4–0.5 reported by de Avillez & Breitschwerdt (2005). This is likely due to the different assumptions in our adopted heating rate. De Avillez & Breitschwerdt (2004, 2005) chose their diffuse heating rate to balance cooling at $T = 9000$ K in the midplane in the initial condition; our heating rate, set directly from Wolfire et al. (1995), is only 57% of the cooling rate in the midplane in the initial condition, $n_0 = 1.29$ cm^{-3}. In our model, $n_0\Gamma = n_0^2\Lambda(T)$ at $T \approx 1301$ K, so gas at 2000 K $< T <$ 9000 K will cool to the cold branch in our model but heat to the warm branch in de Avillez & Breitschwerdt (2004, 2005) if not disturbed by warmer or cooler gas or a shock. Note that the heating rate in de Avillez & Mac Low (2002) and subsequent works is ≈1.7 times the heating rate employed in our model at $T = 9000$ K, not 18 times larger as noted in Joung et al. (2009) and Hill et al. (2012) (M. Avillez 2012, private communication).

Because the remaining figures and conclusions are very similar in the revised runs compared to the original runs, we do not reproduce them here.

The authors thank Erica Rosenblum for identifying the error in the code.

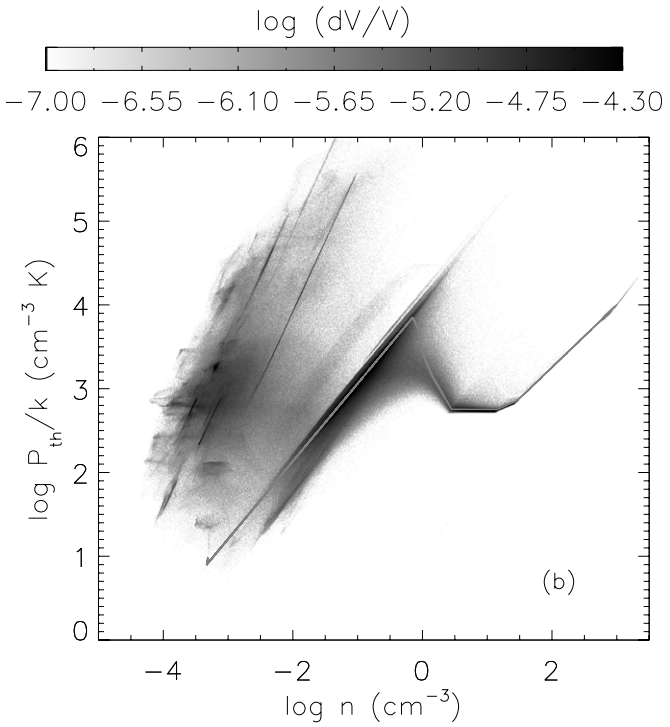

Figure 14. Phase diagram of thermal pressure (nT) as a function of density, calculated for every cell in the range $|z| < 20$ pc in a snapshot of the revised `bx50hr` model at 310 Myr. The gray line shows the curve of thermal equilibrium ($n^2\Lambda = n\Gamma$) for our cooling curve and diffuse heating function at $z = 0$ for $T < 2 \times 10^4$ K.

REFERENCES

de Avillez, M. A., & Breitschwerdt, D. 2004, A&A, 425, 899
de Avillez, M. A., & Breitschwerdt, D. 2005, A&A, 436, 585
de Avillez, M. A., & Mac Low, M.-M. 2002, ApJ, 581, 1047
Ferrière, K. M. 2001, RvMP, 73, 1031
Hill, A. S., Joung, M. R., Mac Low, M.-M., et al. 2012, ApJ, 750, 104
Joung, M. R., Mac Low, M.-M., & Bryan, G. L. 2009, ApJ, 704, 137
Reynolds, R. J., Haffner, L. M., & Tufte, S. L. 1999, ApJ, 525, L21
Wolfire, M. G., Hollenbach, D. J., McKee, C. F., Tielens, A. G. G. M., & Bakes, E. L. O. 1995, ApJ, 443, 152